Anatase TiO 2 Nanocomposites for Antimicrobial Coatings

ARTICLE *in* THE JOURNAL OF PHYSICAL CHEMISTRY B · JUNE 2005

Impact Factor: 3.3 · DOI: 10.1021/jp0502196 · Source: PubMed

3 AUTHORS, INCLUDING:

Patricia S Vary
Northern Illinois University
32 PUBLICATIONS **996** CITATIONS
SEE PROFILE

Chhiu-Tsu Lin
Northern Illinois University
118 PUBLICATIONS **1,365** CITATIONS
SEE PROFILE

Anatase TiO_2 Nanocomposites for Antimicrobial Coatings

Guifen Fu, Patricia S. Vary, and Chhiu-Tsu Lin*

Department of Chemistry and Biochemistry, Northern Illinois University, DeKalb, Illinois 60115-2862

Received: January 12, 2005; In Final Form: March 2, 2005

A sol−gel chemistry approach was used to fabricate nanoparticles of TiO_2 in its anatase form. The particle size is shown to be sensitive to the use of $HClO_4$ or HNO_3 as acid catalyst. The gold-capped TiO_2 nanocomposites were processed by the reduction of gold on the surface of the TiO_2 nanoparticles via a chemical reduction or a photoreduction method. Different percentages of vanadium-doped TiO_2 nanoparticles, which extended the TiO_2 absorption wavelength from the ultraviolet to the visible region, were successfully prepared. The synthesized nanocomposites have a size of about 12−18 nm and an anatase phase as characterized by XRD, TEM, AFM, and UV−vis spectroscopy. The TiO_2 nanocomposite coatings have been applied on glass slide substrates. The antibacterial activity of TiO_2 nanocomposites was investigated qualitatively and quantitatively. Two types of bacteria, *Escherichia coli* (DH 5α) and *Bacillus megaterium* (QM B1551), were used during the experiments. Good inhibition results were observed and demonstrated visually. The quantitative examination of bacterial activity for *E. coli* was estimated by the survival ratio as calculated from the number of viable cells, which form colonies on the nutrient agar plates. The antimicrobial efficiency and inhibition mechanisms are illustrated and discussed.

1. Introduction

The TiO_2 photocatalysts have been investigated extensively for the killing or growth inhibition of bacteria.[1−3] Most works have been done by using a fine TiO_2 powder and a strong UV light. Only a little work has been reported in the use of TiO_2 nanoparticle aqueous solutions coated on substrates.[4,5] Recently, nanosize (<100 nm) TiO_2 particles have attracted a lot of activity from many researchers.[6] These nanometer-size TiO_2 particles exhibit many special properties due to the fact that the band gap of the nanoparticles increases with the decrease of their size, and the small TiO_2 particles offer a very large surface area.[7−9]

When TiO_2 catalyst is irradiated with light of energy greater than or equal to its band gap energy, electron−hole pairs are generated that can induce redox reactions at the surface of the TiO_2.[10] The general scheme for the photocatalytic damage of microorganism cells by TiO_2 photocatalytic properties involves several steps:[11] (1) the photoexcited TiO_2 catalyst produces electron−hole pairs that migrate to the TiO_2 surface; (2) photogenerated holes in TiO_2 can react with adsorbed H_2O or OH^- at the catalyst/water interface to produce the highly reactive hydroxyl radicals and the electrons can react with oxygen vacancies to form superoxide ions; (3) finally, the various highly active oxygen species generated can oxidize organic compounds/cells adsorbed on the TiO_2 surface, resulting in the death of the microorganisms.

The efficiency of TiO_2 photocatalytic properties and antibacterial activities should depend on our abilities (i) to make stable nanostructured TiO_2 particles or composites, (ii) to generate electron−hole pairs by extending the excitation wavelength to the visible light region, and (iii) to achieve a reduced recombination rate on the newly created electron−hole carriers. Several methods may be used to improve the photocatalytic efficiency, including increase of the surface area of TiO_2 through tailoring particle size and pore-size distributions, generation of defect structures to induce space-charge separation via metal dopants, and surface modification of the TiO_2 with a metal or another semiconductor.[12−14] Because the majority of photoexcited charge carriers [electrons (e^-) and holes (h^+)] may undergo a rapid recombination, single component semiconductor nanoparticles have shown to exhibit relatively poor photocatalytic efficiency. Semiconductor−metal nanocomposites, on the other hand, exhibit increased efficiency of photocatalytic activity because of a reduction in the e^-−h^+ recombination rate due to better charge separation between the electrons, which accumulate on the metal, and holes, which remain on the photocatalyst surface. Many investigations have reported that the addition of noble metals such as gold and silver may enhance the overall photoefficiency of TiO_2, and a variety of noble metal capped TiO_2 nanocomposite solutions have been synthesized in recent years to improve the efficiency of the photocatalytic activity of TiO_2.[15]

In this paper, an anatase phase TiO_2 nanoparticle suspension, a gold-capped TiO_2 nanocomposite aqueous solution, and vanadium-doped TiO_2 nanoparticles in aqueous solution are processed by a sol−gel technique and dispersed to form coatings that can inhibit microbial growth on various substrates. The TiO_2 nanoparticles and nanocomposites were characterized by X-ray diffractometry (XRD), transmission electron microscopy (TEM), UV−vis absorption spectroscopy, and atomic force microscopy (AFM). The antibacterial effect of those nanoparticle suspensions and coatings were investigated, both qualitatively and quantitatively, using *Escherichia coli* (DH 5α), a Gram-negative bacterium, and *Bacillus megaterium* (QM B1551), a Gram-positive bacterium.

2. Experimental Section

2.1. Materials. Titanium(IV) isopropoxide (98%) was purchased from Strem Chemical Company and used as received.

* To whom correspondence should be addressed. Telephone: (815) 753-6861. Fax: (815) 753-4802. E-mail: ctlin@niu.edu.

10.1021/jp0502196 CCC: $30.25
Published on Web 03/31/2005

Sodium borohydride (powder, 98%), hydrogen tetrachloroaurate-(III) trihydrate, and ammonium metavanadate (99%) were obtained from Aldrich Chemical. 1-Propanol (anhydrous, 99.7%) was obtained from Sigma-Aldrich. Ethyl alcohol, 200 proof, was purchased from Pharomco. The water employed in all preparations was purified by a Milli-Q system (Millipore). Two bacteria strains, *Bacillus megaterium* (QM B1551) and *Escherichia coli* (DH 5α), were from laboratory stock of the Biological Sciences Department of Northern Illinois University. Other materials for bacteria cultivation, such as agar, yeast extract, sodium chloride, tryptone, and plastic and Pyrex Petri dishes were used from conventional laboratory stock.

2.2. Preparation of TiO_2 Nanoparticle/Nanocomposite Aqueous Colloidal Solution and Coating. Different concentrations of TiO_2 nanoparticle aqueous solution were prepared by the procedure described previously.[16] As an example, for 5 mM TiO_2 nanoparticle suspensions, 0.5 mL of titanium isopropoxide was added to 4.5 mL of 1-propanol to achieve a 10% titanium isopropoxide solution. In a separate beaker, 200 mL of deionized water was adjusted to a pH ~1.5 with 6 M $HClO_4$ or HNO_3. Then, 2.97 mL of 10% titanium isopropoxide was added dropwise to the pH-adjusted water with vigorous stirring using a magnetic stir bar for about 1−1.5 h, resulting in a transparent 5 mM TiO_2 colloidal solution.

The TiO_2/Au nanocomposites were prepared by adding the desired amount of 5 mM stock $HAuCl_4$ solution to the 5 mM colloidal TiO_2 suspension prepared above while stirring vigorously. Reduction of $[AuCl_4]^-$ was achieved by dropwise addition of sodium borohydride (9 mM, in ethanol) until a wine-red color was observed. Two different TiO_2/Au solutions were prepared containing a $[TiO_2]$:[Au] ratio of 20:1 (a wine-red color) and 1:1 (a dark purple color) by keeping the gold concentration constant at 0.2 mM while varying the TiO_2 concentration from 4 to 0.2 mM. The TiO_2/Au nanocomposites were also synthesized by a photoreduction method using a 450 W Xe lamp.

Various concentrations (3−13 wt %) of vanadium-doped TiO_2 nanoparticle solutions were prepared. As an example, for a 3 wt % vanadium-doped TiO_2 nanoparticle solution, 0.02 g of NH_4VO_3 was dissolved in 20 mL of deionized water while stirring and heating slightly for about 10 min. The prepared NH_4VO_3 solution was added dropwise to 20 mL of TiO_2 nanoparticle solution and stirred for about 1 h.

2.3. Characterization of Nanoparticles/Nanocomposites. UV−vis absorption spectra of colloidal solutions were recorded by a Perkin-Elmer double beam scanning spectrometer, Model Lambda 19. The TiO_2 crystal structure of the dry solution (powder) was investigated by Rigaku Miniflex X-ray powder diffraction (XRD). The white powder was obtained from 5 mM TiO_2 solution after slow evaporation of solvents, and was ground and compressed in a sample holder. The XRD pattern was obtained with Cu Kα radiation at 60 keV and 15 mA over the range $20° < 2\theta < 60°$. The morphology and size of the nanoparticles/nanocomposites were studied with a JEOL 2010 transmission electron microscope (TEM) operating at 200 keV and 110 μA equipped with a Gatan CCD camera, and a Quesant Q-scope 2350 atomic force microscope (AFM). Different area sizes of the sample surfaces were scanned with 600 × 600 pixel scan resolution to make a complete contour of the sample.

2.4. Bacterial Cultures and Test of Antibacterial Activities. Two types of bacteria, *B. megaterium* (QM B1551), a Gram-positive bacterium, and *Escherichia coli* (DH 5α), a Gram-negative bacterium, were used as model bacteria in this study. Luria broth (LB) and agar were used as sources for culturing *E. coli* at 37 °C on a rotary platform in an incubator. The *B. megaterium* was grown in Supplemental Nutrient Broth (SNB) at 30 °C for about 14−16 h. The density of the bacterial cells in liquid cultures was estimated by optical density (OD) at 600 nm wavelength. The OD was chosen in a range of 0.8−1.0, which is the optimal optical density of the cells for conventional bacterial activity testing. The cell suspensions used for antibacterial activity on both solution phase and coated glass substrate were 10^8−10^9 colony-forming units (cfu)/mL.

2.5. Bacterial Activity Test on TiO_2 Nanocomposites in Solution Phase. The following procedures were used for testing antibacterial activity of *E. coli* and *B. megaterium* using TiO_2 nanoparticle solution, gold-capped TiO_2 nanocomposite solution, and vanadium-doped TiO_2 nanocolloid. The testing Petri plates were prepared by LB or SNB medium. Using a homemade glass atomizer, the bacteria were sprayed evenly on the top of the medium covering the whole area of the testing Petri plate. After about 5−10 min to allow the bacteria to dry out, the testing solutions of TiO_2 nanocomposites were dropped on top of the bacteria. For each testing solution, three marked spots on each Petri dish were applied. In this way, the large part of the bacteria was on the culture medium, and three marked areas of the bacteria were on the testing solution. Samples of the testing Petri plates were kept in the incubator at 37 °C for *E. coli* and 30 °C for *B. megaterium* for 20−26 h, and then testing results were determined visually and with the aid of an optical microscope.

2.6. Bacterial Activity Test for TiO_2 Nanocomposites on Coated Glass Substrates. The tests of inhibition of bacterial growth for TiO_2 nanocomposites on coated glass substrates were carried out both qualitatively and quantitatively. In the qualitative testing, the testing glass plate was spray-coated and thermally cured at 90 °C for 30 min on three marked areas using a fixed concentration of TiO_2 nanoparticle solution, gold-capped TiO_2 nanocomposite solution, or vanadium-doped TiO_2 nanocolloid. The coated glass slides were sterilized by autoclaving. The bacteria were sprayed evenly across the entire testing substrate using a small homemade atomizer and allowed to dry for 10 min. The nutrition agar, LB for *E. coli* and SNB for *B. megaterium*, was pipetted onto the top of the bacteria. There are two important steps that need to be done very carefully. One is to spray the bacteria as evenly as possible; the other is to carefully control the temperature of the LB agar when pipetting it onto the bacteria. The melting point of LB agar is 100 °C and it will become a gel at about 45 °C; higher than 55 °C, the bacteria will be killed by the high temperature. Therefore, the optimal temperature to pipet the LB agar is at about 55 °C. Samples of the coated glass plates are then transferred to a clean Petri dish and kept in the incubator at 37 °C for *E. coli* and 30 °C for *B. megaterium* for 20−26 h. The qualitative testing results of bacterial activity were determined visually and with the aid of an optical microscope.

For the quantitative testing, a set of quantitative dilutions of bacteria suspensions were used and the number of bacterial colonies appearing on the coated plates are actually counted under a microscope. Equal aliquots of 1 mL of *E. coli* suspension were pipetted into the TiO_2/Au nanocomposite coating chambers, and then 50 μL of the reaction mixture was immediately taken from the chamber and diluted into 4.95 mL of LB broth in a centrifuge tube to achieve the 10^{-2} colony-forming units (cfu)/mL. The series of dilutions from 10^{-2} cfu/mL of reaction mixture solution was conducted by taking out 50 μL of the 10^{-2} cfu/mL solution and diluting to 10^{-4} cfu/mL with 4.95 mL of LB broth in a centrifuge tube, and then mixing completely. Similarly, a total of four different concentrations, 10^{-4}, 10^{-5},

10^{-6}, and 10^{-7} cfu/mL, of the original concentration of the reaction mixture, were pipetted onto the LB agar plates for each sample, and three replicate plates were used for each dilution. The sample plates were kept in an incubator at 37 °C for about 24 h; the number of viable cells in the sample was determined by choosing the appropriate dilution of the sample onto LB agar plates and counting colonies that appeared on the plates under a microscope. An average number of viable cells was obtained by averaging the numbers in the three replicate plates.

3. Results and Discussion

3.1. Anatase TiO_2 Nanocolloid Suspension. Several methods for synthesizing TiO_2 nanoparticles have been published.[17−22] Two major structural forms of titanium dioxide can exhibit photocatalytic activity: anatase and rutile.[11] Anatase (chains of TiO_6 octahedral sharing two edges) has a wider optical band gap of 3.2 eV, and the band gap of rutile (chains of TiO_6 octahedral sharing four edges) is 3.0 eV.[19] It is important to develop methods for the selective preparation of TiO_2, because anatase and rutile are often formed at the same time during the formation of TiO_2 and it is desired to synthesize anatase nanoparticle TiO_2 since the anatase form has a higher photocatalytic activity than rutile TiO_2.[23]

Different preparation methods and conditions yield different particle sizes and phase compositions of the nanostructured TiO_2 that display different morphological, structural, and surface physiochemical properties, and also give different photocatalytic activities.[24,25] These conditions include the types of precursors, the concentration and molar ratio of reactants, the polarity of the solvent, the pH, and the temperature of the reacting solution.

In this study, we focused on the preparation of highly photoactive nanosize anatase structured TiO_2. The TiO_2 nanoparticle aqueous suspension was prepared by employing titanium isopropoxide as a precursor, water as a solvent, and HNO_3 or $HClO_4$ as a catalyst at room temperature for a period of at least 2 h. This allowed for a hydrolysis reaction to take place and ensured the formation of a transparent TiO_2 solution. The pH of these solutions is about 1.5. At this pH, nanoparticles are positively charged, which favors the formation of small particles. Two different acids, HNO_3 and $HClO_4$, were used for controlling the solution pH. The dropping speed of titanium isopropoxide solution into water had an important effect on the particle size of TiO_2. At room temperature and pH 1.5 and when titanium isopropoxide solution was added dropwise slowly over a period of 1.0−1.5 h, a transparent colloidal solution was obtained. When titanium isopropoxide solution was added dropwise rapidly within 30−40 min, a less transparent or an "opaque" solution was observed. This result indicated that the key parameters for producing small TiO_2 particles in aqueous suspension are the pH of the solution and the rate of addition.

The UV−vis absorption spectrum of a 5 mM TiO_2 nanoparticle solution is shown to have an absorption edge at ∼360 nm (i.e., 3.45 eV), indicating that the TiO_2 colloidal solution obtained is anatase and not rutile. The band gap of the prepared TiO_2 nanoparticles is at a higher energy than that determined for bulk anatase (3.2 eV). Several different concentrations of TiO_2 aqueous suspensions were prepared in an attempt to obtain a TiO_2 nanoparticle solution in a higher concentration. The highest concentration that could be reached in an aqueous suspension was 260 mM. A key factor for preparing an aqueous solution higher than 5 mM TiO_2 is controlling the rate of dropwise addition of the titanium isopropoxide solution into the water by slowly adding titanium isopropoxide into water, drop by drop, much more slowly than when making the 5 mM TiO_2 solution, while lowering the temperature with an ice bath (at ∼4 °C) to obtain a transparent solution. In trying to make a solution concentration higher than 260 mM TiO_2 aqueous suspension, white suspensions were immediately formed upon addition of titanium isopropoxide solution to the water. X-ray diffraction (XRD) was used to investigate the crystalline phases (anatase or rutile) of the TiO_2 powder. Two different acids used to control the pH in preparing 5 mM TiO_2 nanoparticle suspension were then investigated. Figure 1 shows the XRD pattern of TiO_2 powder made by hydrolysis of titanium isopropoxide with different acids, either HNO_3 or $HClO_4$. The XRD shows that both acids yield the anatase phase of TiO_2. The type of acid used in this synthesis gives an identical anatase phase of titanium dioxide with this preparation method. As illustrated, two syntheses gave the same structures in the XRD pattern: broad peaks are observed at values of 2θ equal to 25.5, 38.5, 48.2, 54.4, and 55.4° that correspond to the anatase structure.[18] A small broad signal at 31° is from TiO_2 brookite. Also, strong peaks are observed at 38.3 and 45° that are attributed to the diffraction of aluminum, which is the sample holder. A good match of peaks from the TiO_2 sample spectra with a library spectrum of anatase TiO_2 is shown in the bottom of Figure 1. It further confirms that TiO_2 nanoparticles prepared by this method, with either HNO_3 or $HClO_4$ acid, both generate an anatase crystalline structure without a significant amount of any other phase. From the diffraction patterns, the anatase TiO_2 materials prepared are in the form of very small particles, since the XRD peaks are very broad.

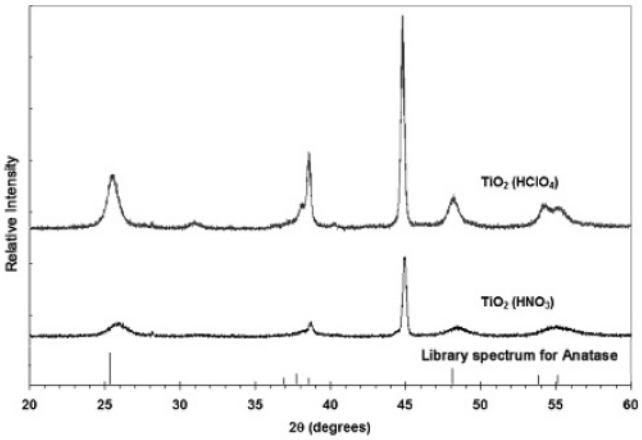

Figure 1. XRD pattern of TiO_2 nanoparticles prepared by the hydrolysis of titanium isopropoxide, and catalyzed by either HNO_3 or $HClO_4$. A library spectrum of anatase TiO_2 is marked for comparison.

The morphology and size of the colloidal nanoparticles were examined by TEM. The TEM image of 5 mM TiO_2 nanoparticles is presented in Figure 2. A TiO_2 particle size of about 12−18 nm was obtained, and a spherical particle shape of anatase TiO_2 was also observed. To further characterize the TiO_2 nanoparticles, the AFM was used to examine the morphology of the coating. A 5 mM TiO_2 aqueous solution, prepared with either HNO_3 or $HClO_4$ acid, was coated on window glasses and examined. The left and right portions of Figure 3 show the AFM angle view image and top view image of 5 mM TiO_2 nanoparticles coated on glass, respectively, when $HClO_4$ acid was used in the synthesis of TiO_2 suspension. From these images, small particles were observed and their dimension varied in a narrow range (40−100 nm); the shape of the particles was almost spherical. A similar result was also obtained from 5 mM TiO_2 nanoparticles coated on glass prepared with HNO_3 acid. The AFM angle view image (left) and top view image (right) are shown in Figure 4. The AFM images again prove that the

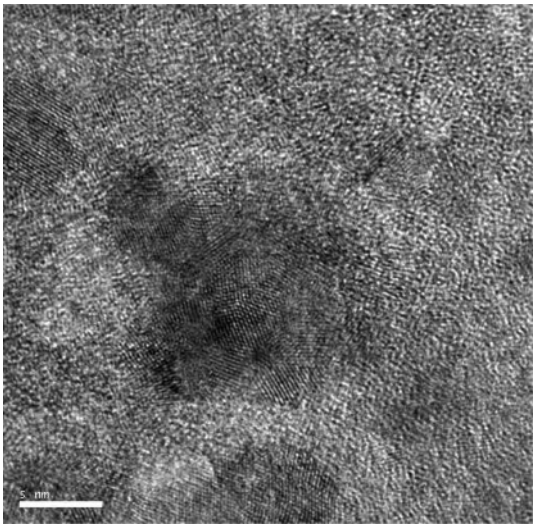

Figure 2. TEM image of 5 mM TiO_2 nanoparticle suspension.

same structure of TiO_2 nanoparticles was obtained by using both acids. However, the images show that the particle size is a little smaller when prepared with HNO_3 (<50 nm) than that with $HClO_4$ (<100 nm) acid.

The TiO_2 particle size is smaller according to the TEM results than with the AFM image, which may reflect the drying-induced particle growth or aggregating. For the AFM imaging, the coated glasses were dried at room temperature for 1 week, and then at 90 °C in an oven for about 1/2 h. For TEM measurement, the freshly prepared solutions were used; the sample preparation for TEM testing requires an overnight drying process.

3.2. Formation of Gold-Capped TiO_2 Nanocomposites. Gold can be deposited on the TiO_2 nanoparticle surface by either cation adsorption or anion adsorption to the TiO_2 surface depending on the pH of the working solution. The TiO_2 is an amphoteric oxide with an isoelectric point[26] $IEP_{TiO_2} = 6$. Therefore, when the solution pH is higher than IEP_{TiO_2}, the main surface species is $-O^-$, so the TiO_2 surface is negatively charged and gold can be deposited on TiO_2 by cation adsorption. When the solution pH is lower than IEP_{TiO_2}, the main surface species is $-OH_2^+$, so the TiO_2 surface is positively charged. Then gold can be produced on the TiO_2 surface by anion adsorption. For example, gold-capped TiO_2 can be prepared by adding the desired amount of $HAuCl_4$ solution to the colloidal TiO_2 solution made in an acidic medium while stirring vigorously. The TiO_2 colloids prepared in acidic media are positively charged. They act as a support to adsorb $[AuCl_4]^-$. The negatively charged $[AuCl_4]^-$ adsorbs strongly on the TiO_2 nanoparticle surface. Upon reduction with $NaBH_4$, stable TiO_2/Au nanocomposites are obtained in aqueous solution. Gold actually covers only a small area of the TiO_2 surface. Therefore, a large surface area of TiO_2 nanoparticle is still exposed. Gold reduction carried out in the absence of a TiO_2 core using the same experimental procedure and conditions did not produce stable colloids.[27]

Two methods are used to prepare TiO_2/Au nanocomposite solutions: chemical reduction and photoreduction. The gold-capped TiO_2 nanoparticles were prepared by first synthesizing TiO_2 nanoparticle suspensions in aqueous solution (stabilized at pH 1.5) and then capping these particles with gold nanocrystallites. In acidic medium, when the noble metal salt ($HAuCl_4$) solution was added to the TiO_2 aqueous solution, the

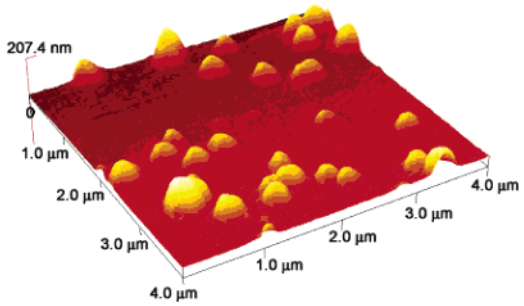

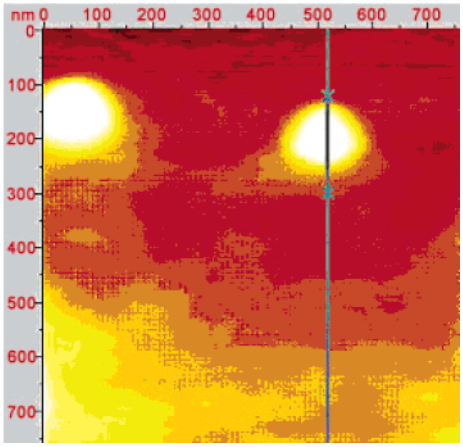

Figure 3. (left) AFM angle view image and (right) AFM top view image, of 5 mM TiO_2 nanoparticles catalyzed by $HClO_4$ and coated on glass.

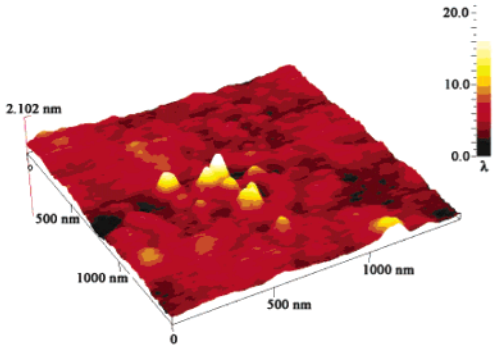

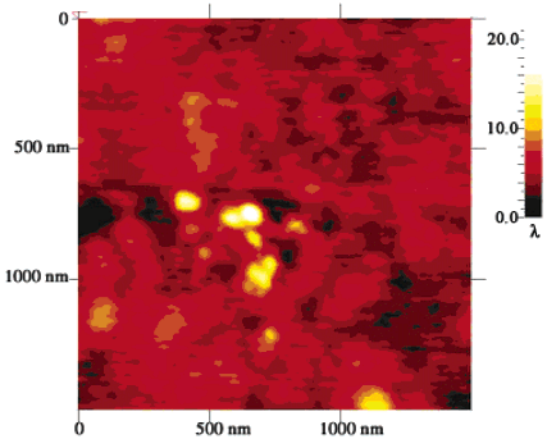

Figure 4. (left) AFM angle view image and (right) AFM top view image, of 5 mM TiO_2 nanoparticles catalyzed by HNO_3 and coated on glass.

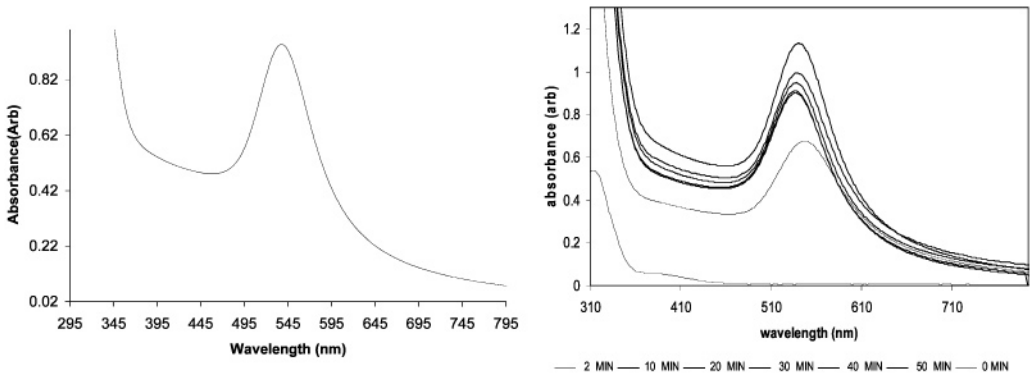

Figure 5. UV−vis absorption spectra of Au-capped TiO_2 nanocomposites (a $[TiO_2]$:[Au] ratio of 20:1): (left) reduced by $NaBH_4$ and (right) reduced by UV irradiation of different exposure times.

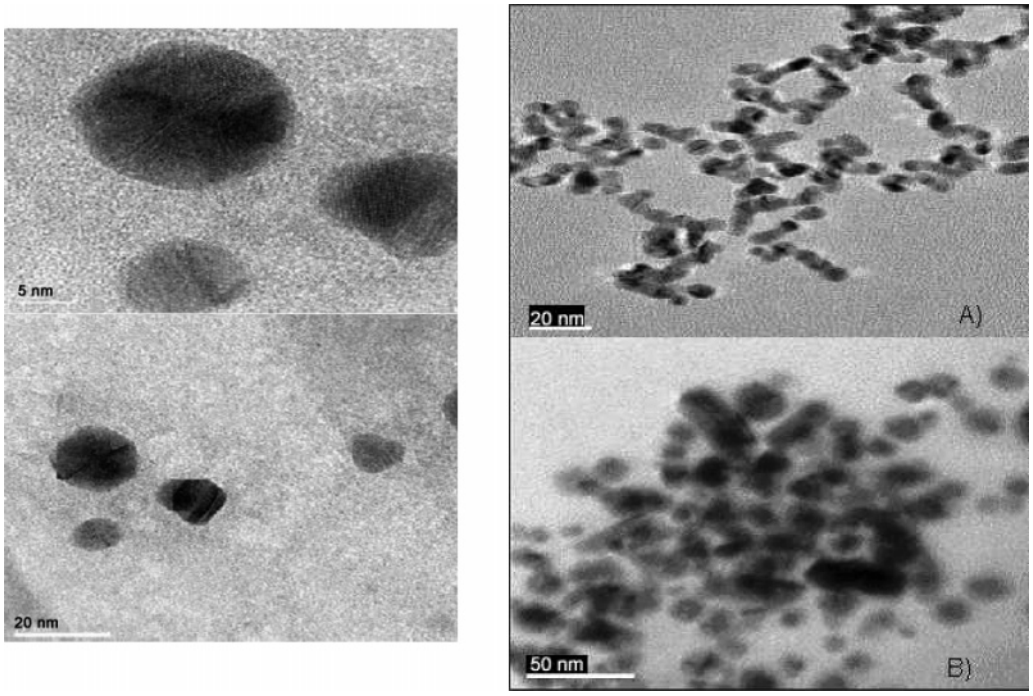

Figure 6. TEM images: (left) 4 mM gold-capped TiO_2 nanocomposites; (right) TiO_2/Au nanocomposites at different $[TiO_2]$:[Au] ratios of (A) 20:1 and (B) 1:1.

TiO_2 core acted as a support to adsorb $[AuCl_4]^-$ ions first. Then, upon reduction with a freshly prepared solution of $NaBH_4$, stable TiO_2/Au nanocomposites were obtained and the aqueous solution was wine-red in color. A broad spectral band at 537 nm, which is attributed to the surface plasmon band of gold nanoparticles,[27] appears on the UV−vis absorption spectrum of Au-capped TiO_2 suspension as shown in the left portion of Figure 5.

The transmission electron micrograph (TEM) of gold-capped TiO_2 nanocomposite is shown in the left portion of Figure 6. A well-defined image of spherical shape of TiO_2/Au nanocomposites was obtained. The particle diameter of gold-capped TiO_2 nanocomposites was in the range of 10−15 nm, almost the same size as TiO_2 nanoparticles alone. Compared to the TEM graph of TiO_2 nanoparticles, shown in Figure 2, there is no significant change in particle size, indicating that the TiO_2 surface was capped with a very thin shell or islands of gold, so the size was determined by the TiO_2 nanoparticles.

Two different ratios of $[TiO_2]$:[Au] nanocomposite solutions were prepared and characterized. Transmission electron micrographs of two different $[TiO_2]$:[Au] ratios are shown in the right portion of Figure 6. For the high core:shell ratio (i.e., a $[TiO_2]$:[Au] ratio of 20:1), fairly uniform size gold-capped TiO_2 nanocomposites of about 5−10 nm diameter were obtained (image A). In contrast, the TEM image for the $[TiO_2]$:[Au] ratio of 1:1 nanocomposites showed a larger size of about 10−20 nm (image B). They also tend to close in on each other, indicating the aggregation effect. The fact that the optimal amount of Au was obtained at relatively low loading or at relatively low surface coverage of TiO_2 may reflect some recombinative activity of the metallic islands.[11] Without Au-capped particles, TiO_2 solutions showed significant turbidity after several hours at room temperature. In contrast, the TiO_2/Au solution remained clear, indicating that gold capped the TiO_2 particles and protected them against precipitation. Therefore, the 4 mM TiO_2/Au solution with a $[TiO_2]$:[Au] ratio of 20:1 was chosen as the one of the testing solutions for antibacterial study in this study.

The reduction of $[AuCl_4]^-$ ions absorbed on the surface of TiO_2 particles can also be done photochemically. The right portion of Figure 5 shows the absorption spectra of Au-capped TiO_2 nanocomposites prepared by using the photoreduction method at different UV exposure times. No coloration change took place at the zero exposure time, and no Au surface plasmon band was observed in the absorption spectra. When the TiO_2 with $HAuCl_4$ mixture solution was exposed to UV light, after

2 min exposure time, the gold was reduced on the surface of TiO_2, which was confirmed by UV−vis absorption spectra. The λ_{max} values were observed in the range 537−543 nm, indicating the formation of Au(0) nanoparticles. Under UV irradiation, TiO_2 nanoparticles undergo charge separation,[27] and the generated electron−hole carriers can act to reduce $[AuCl_4]^-$ ions that produce TiO_2/Au nanocomposites via the following mechanisms:

$$TiO_2 + h\nu \rightarrow TiO_2\,(h^+ + e^-) \quad (1)$$

$$TiO_2\,(3e^-) + Au^{3+} \rightarrow TiO_2 + Au^0 \quad (2)$$

Chlorine atoms produced during the reactions presumably reacted with water to form hydrochloric acid and hypochlorous acid.

3.3. Generation of Vanadium-Doped TiO_2 Nanocolloid. To initiate photocatalytic reaction, a light source with energy greater than the TiO_2 band gap energy is required. The band gap energy of TiO_2 is high in the UV range of less than 385 nm. This limitation has been overcome by doping various transition metal ions into TiO_2, to extend the excitation wavelength range of TiO_2 from the UV into the visible region where convenient light sources are available.[28,29] The primary process is that the transition metal ions absorb light in the visible region and transfer the excited electron to the TiO_2 conduction band. For example, in one study,[28] titanium tetraisopropoxide was used as a titanium dioxide source; NH_4F was used as a precursor of the dopant. The F^--doped TiO_2 with anatase and brookite phases was synthesized by hydrolysis of titanium tetraisopropoxide in an NH_4F aqueous solution. The result showed that the F^--doped TiO_2 samples exhibited strong absorption in the UV−visible range and a red shift in the band gap transition. Another research group, Klosek et al., studied TiO_2 particles doped with V^{4+} and found that V^{4+}-doped TiO_2 has the effect of extending the wavelength range of the TiO_2 into the visible region (396−450 nm).[30] The advantages of transition metal doping include extending the wavelength to the visible region and also improving the photocatalytic activity of the TiO_2. It is noted[29] that some research results showed certain metals such as Fe^{3+} and V^{4+} in Fe^{3+}- and V^{4+}-doped TiO_2 actually reduced the electron−hole pair recombination rate and improved the photocatalytic activity over the undoped TiO_2. Some metal ions such as Co^{3+} and Al^{3+} in Co^{3+}- and Al^{3+}-doped TiO_2 either showed no improvement or even decreased the photocatalytic efficiency of TiO_2.[29]

A series of vanadium-doped TiO_2 nanocolloids have been synthesized and investigated. The absorption spectra of TiO_2 particles doped with different percentages of vanadium are shown in Figure 7. Without vanadium doping, the UV−vis absorption spectrum of a 5 mM anatase TiO_2 nanoparticle solution is shown to have an absorption edge at ~360 nm (i.e., 3.45 eV). The absorption edge of vanadium-doped TiO_2 nanocolloids is progressively red shifted with vanadium concentration. A red shift to the visible region at 450 and 500 nm is shown in Figure 7 for a 3% and 7% V-doped TiO_2 nanocolloid, respectively. There was no further red shift at concentrations higher than 7% V-doped TiO_2 solution.

3.4. Bactericidal Activity Effect on TiO_2 Nanocolloid Solutions. The bactericidal activities of the anatase TiO_2 nanocomposites were evaluated by the inhibition of bacterial growth of *B. megaterium* and *E. coli*. *B. megaterium* is one of the Gram-positive bacteria and *E. coli* is one of the Gram-negative bacteria. The Gram-positive bacteria have a relatively

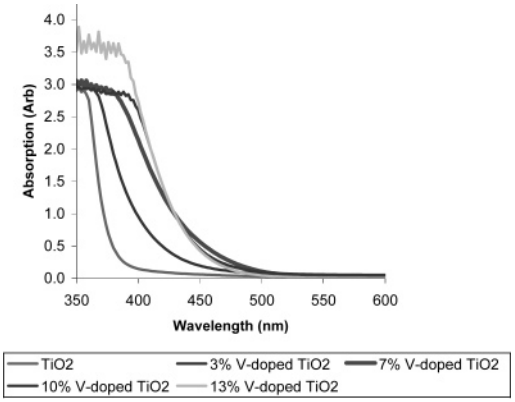

Figure 7. Absorption spectra of different percentages of V-doped TiO_2 nanoparticle suspension.

thick wall composed of many layers of peptidoglycan polymer, and only one membrane (plasma membrane). The Gram-negative bacteria have only a thin layer of peptidoglycan and a more complex cell wall with two cell membranes, an outer membrane, and a plasma membrane. The addition of the outer membrane of the Gram-negative bacteria cells influences the permeability of many molecules. Under certain conditions, the Gram-negative bacteria are more resistant to many chemical agents than Gram-positive cells.[31]

The photocatalytic process of anatase TiO_2 particles includes chemical steps that produce highly reactive species such as hydroxyl radical, hydrogen peroxide, and superoxides that, in principle, can cause fatal damage to microorganisms.[4] Among these reactive oxygen species, the hydroxyl radicals are highly reactive and therefore short-lived. The superoxide ions are relatively longer lived. Due to their negative charge they cannot penetrate the cell membrane. They must contact directly the outer surface of bacteria unless the TiO_2 particle has penetrated the cell. Hydrogen peroxide is less harmful compared to hydroxyl radicals and superoxide ions, but it can enter the cell.[32] However, among these reactive oxygen species, which species are directly involved in the damage of bacterial cells or which species contribute more to the oxidative reactions with organic compounds is still subject to investigation.

Several proposed mechanisms for cell killing by the TiO_2 photocatalytic processes were reported.[4,33] The Sunada research group reported[32] direct evidence of cell membrane damage by the irradiation of a thin transparent TiO_2 film to examine the photocatalytic degradation of endotoxin from *E. coli*. The endotoxin is a component of the outer membrane of Gram-negative bacteria and is released only when the cellular structure is destroyed. The results indicated that the TiO_2 photocatalyst destroys the outer membrane of the *E. coli* cell and causes the death of the bacteria.[4] Recently, the mechanism of cell killing of *E. coli* on TiO_2 thin films has been investigated by atomic force microscopy (AFM).[33] The damage process of the cell wall and the cell membrane was observed by AFM imaging. Also, the permeability of the cell membrane was examined by K^+ leakage from *E. coli*. Results showed that the intracellular K^+ leaked out from *E. coli* very quickly after TiO_2 thin film was irradiated by UV. The researchers believe the cell death was caused by the decomposition of the cell wall first, and then subsequent decomposition of cell membrane.[33] Damage of the cell membrane directly leads to leakage of minerals, proteins, and genetic materials, causing cell death.

In this paper, the antibacterial effect of nanocomposites on *E. coli* and *B. megaterium* was first tested for TiO_2 suspensions and gold-capped TiO_2 solutions. A control solution was also

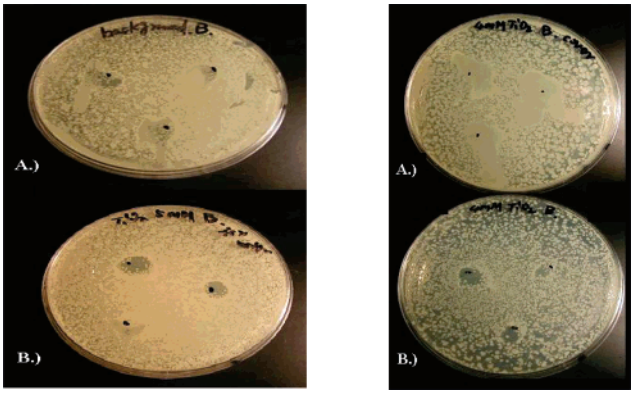

Figure 8. Antibacterial effect on *B. megaterium*. Left: (A) control solution without TiO_2 nanoparticles; (B) 5 mM TiO_2 nanoparticle suspension. Right: 4 mM TiO_2 nanoparticle suspension, (A) dark control covered with an aluminum foil and (B) under room light.

TABLE 1: Antibacterial Effects with Different Concentrations of TiO_2 Suspension on *B. megaterium* and *E. coli*

	5 mM	1 mM	0.5 mM	0.1 mM	0.05 mM	0.01 mM
E. coli	++	−	−	−	−	−
B. megaterium	++	++	+	−	−	−

prepared that contains all other chemical compositions as a 5 mM TiO_2 suspension, but no TiO_2 nanoparticles. The left portion of Figure 8 shows the antibacterial effect on *B. megaterium* using a control solution without TiO_2 nanoparticles (top) and a 5 mM TiO_2 solution (bottom). The result shows that there was no inhibition on bacterial growth when a control solution contains no TiO_2 nanoparticles. On the bottom plate where three spots of 5 mM TiO_2 solution were applied, bacteria grew on the entire plate except those three TiO_2 spots, which display bacteria-free areas compared to the surrounding areas. The antibacterial effect of nanocomposites on *E. coli* and *B. megaterium* was then tested for TiO_2 suspensions with and without room light (fluorescent discharge tubes). The dark sample was carried out by covering the testing plate with aluminum foil. The right portion of Figure 8 shows the antibacterial activity of 4 mM TiO_2 solution on *B. megaterium*, where the top plate was covered with aluminum foil and the bottom plate was not. The results indicate that the antibacterial effects observed in Figure 8 are due to the photocatalytic activity of the TiO_2 nanoparticles in suspension.[4,32]

Under room light condition, a series of dilutions with 5 mM TiO_2 solution was used to examine the concentration effect of TiO_2 suspensions on the antibacterial activity for both *B. megaterium* and *E. coli*. Six different concentrations of TiO_2 suspension were tested, and the results are summarized in Table 1, where "++" indicates the best inhibition results, "+" means relatively less inhibition effect, and "−" represents no inhibition at all. At a 5 mM concentration, TiO_2 suspension inhibits effectively the bacteria growth for both *B. megaterium* and *E. coli*. The inhibition of *B. megaterium* growth activity by TiO_2 suspension is effective in the following order: 5 mM $\approx$ 1 mM $>$ 0.5 mM. No significant antibacterial activity was observed for *B. megaterium* and *E. coli* at of TiO_2 suspension concentrations of 0.1 and 1 mM, respectively. A concentration of TiO_2 suspension an order of magnitude higher is required to kill *E. coli* than to kill *B. megaterium*, probably related to their different cell wall structures and cell membranes. *B. megaterium* is a Gram-positive bacterium with only one membrane, so *B. megaterium* is more sensitive to the chemical agents than *E. coli*, which has a more complex cell wall with two cell

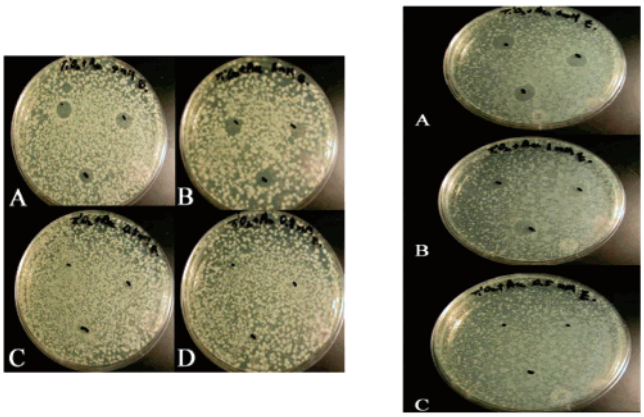

Figure 9. Antimicrobial activity testing with different concentrations of gold-capped TiO_2 nanocomposite solutions. Left: on *B. megaterium* at (A) 4, (B) 1, (C) 0.5, and (D) 0.1 mM. Right: on *E. coli* at (A) 4, (B) 1, and (C) 0.5 mM.

TABLE 2: Antibacterial Effects with Different Concentrations of TiO_2/Au Suspension on *B. megaterium* and *E. coli*

	5 mM	1 mM	0.5 mM	0.1 mM	0.05 mM	0.01 mM
E. coli	++	+	−	−	−	−
B. megaterium	++	++	+	−	−	−

membranes. It is noted that the biological organisms are killed by various highly reactive oxygen species (hydroxyl radical, hydrogen peroxide, or superoxides) generated upon the photocatalytic process of TiO_2 nanoparticle suspension. The antibacterial effects of TiO_2 suspension on both *B. megaterium* and *E. coli* should also be related to the particle size (10−15 nm), surface area, band gap energy (3.45 eV), and coordination of Ti^{4+} ions (tetrahedral) of anatase nanoparticles prepared.

Similar antimicrobial activity testing with different concentrations of gold-capped TiO_2 solutions and V-doped TiO_2 solutions was also performed. The test results with TiO_2/Au nanocomposite solutions on *B. megaterium* and *E. coli* are shown in the left portion and right portion of Figure 9, respectively. The good antibacterial growth of *B. megaterium* is observed for 4 mM (left A) and 1 mM (left B) TiO_2/Au nanocomposite solutions. Some inhibition effect is still observed at a low concentration of 0.5 mM (left C), and no noticeable inhibition effects are seen in the left D plate of Figure 9. For the antibacterial activity of *E. coli*, the TiO_2/Au nanocomposite solutions show good, medium, and no inhibition effects at 5 mM (right A), 1 mM (right B), and 0.5 mM (right C), respectively. The testing results for a wide range of concentrations of TiO_2/Au nanocomposite solutions both bacteria are summarized in Table 2. The antibacterial effects on *B. megaterium* and *E. coli* by TiO_2/Au nanocomposite solutions (Table 2) are shown to be similar to those by TiO_2 nanoparticle solutions (Table 1). However, a slightly better inhibition of bacterial growth is noticed for TiO_2/Au nanocomposite solutions than for TiO_2 nanoparticle solutions. A clear inhibition effect on *E. coli* is observed for the 1 mM TiO_2/Au solution, but not for the 1 mM TiO_2 solution. Moreover, the bacterial inhibition spots on TiO_2/Au nanocomposite testing plates in Figure 9 are much clearer than those spots on TiO_2 nanoparticle testing plates. Table 3 shows the summary of antibacterial activity of *B. megaterium* and *E. coli* by V-doped TiO_2 solutions that are quite similar to those displayed in Tables 1 and 2.

3.5. Bactericidal Activity Effect on TiO_2 Nanocoatings. As shown in the Experimental Section, the TiO_2 nanocomposite coatings were prepared on glass slides for both qualitative and

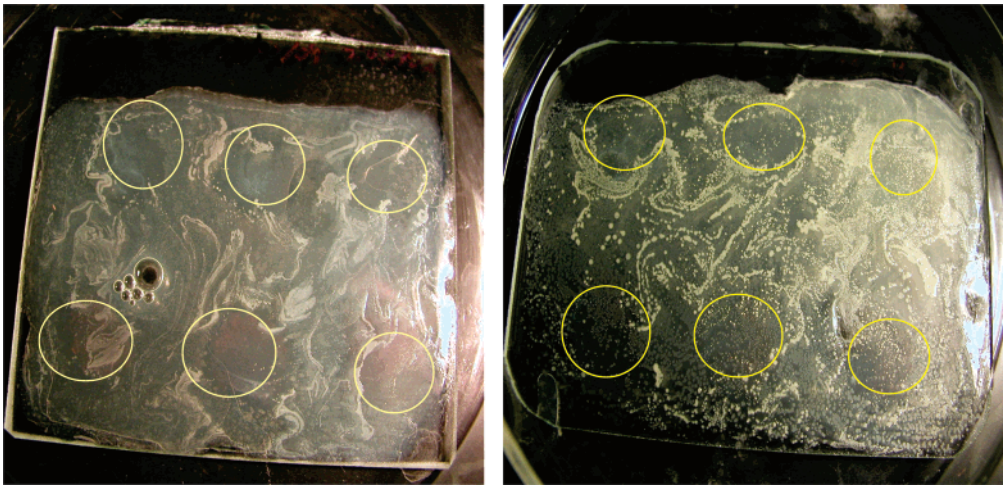

Figure 10. Inhibition growth of *E. coli* (left plate) and *B. megaterium* (right plate). On each plate, the top three circles are coated with 5mM TiO_2 nanoparticles and the bottom three circles are coated with 4 mM TiO_2/Au nanocomposites.

TABLE 3: Antibacterial Effects with Different Concentrations of V-Doped TiO_2/Au suspension on *B. megaterium* and *E. coli*

	5 mM	1 mM	0.5 mM	0.1 mM	0.05 mM	0.01 mM
E. coli	++	+	−	−	−	−
B. megaterium	++	++	−	−	−	−

quantitative testing of antimicrobial activity of *E. coli* and *B. megaterium*. For the qualitative testing, the coated glass slide on the left of Figure 10 shows inhibition of *E. coli* growth with three 5mM TiO_2 nanoparticle coating spots on the top and three 4 mM TiO_2/Au nanocomposite coating spots on the bottom. The circles were marked to indicate where the spray-coat spots were made. As can be seen around the coated spots, there is less growth or no growth of bacteria than in the surrounding uncoated area. Similar results were also obtained for *B. megaterium*, shown on the coated glass slide on the right of Figure 10. Moreover, Figure 11 shows the antibacterial testing for *E. coli* on coated glass slide sprayed by different nanocomposites. The top-left two spots were coated by 5 mM TiO_2 nanoparticle solution, the top-right two spots were made by 4 mM TiO_2/Au nanocomposite solution, the middle-left two spots were coated by 260 mM TiO_2 nanoparticle solution, the middle-right two spots were made by 260 mM TiO_2/Au nanocomposite solution, the bottom-left two spots were identical to (or a repeat of) those on the middle-left two spots made by 260 mM TiO_2 nanoparticle solution, and the bottom-right two spots were coated by 260 mM TiO_2/Ag nanocomposite solution. The results may be summarized as follows: (1) The two spots on the top right, which are coated by 4 mM TiO_2/Au nanocomposite solution, show excellent inhibition results. (2) Comparing the 5 mM TiO_2 coated spots (top-left two spots) and the 260 mM TiO_2 coated spots (middle-left or bottom-left two spots), the lower concentration (or smaller particle size) of TiO_2 nanoparticle exhibits better bacterial inhibition results. (3) Both the 260 mM TiO_2/Au nanocomposite solution (middle-right two spots) and the 260 mM TiO_2/Ag nanocomposite solution (bottom-right two spots) show a similar bacterial inhibition effect.

For the quantitative testing, the survival ratio of *E. coli* cells dropped onto a TiO_2/Au coating was examined as a function of UV illumination time. The light exposure was done either under room light or with a low power LED device emitting at 360, 390, or 470 nm. Two sets of experiments were made, and the results are plotted in Figure 12. In set I, the bacterial suspensions of *E. coli* cells in concentrations of 10^{-2}, 10^{-3}, 10^{-4}, 10^{-5}, 10^{-6}, and 10^{-7} cfu/mL were used for counting a smaller number of survival cells; in set II, the bacterial suspensions of *E. coli* cells in concentrations of 10^{-2}, 10^{-3}, 10^{-4}, and 10^{-5} cfu/mL were used for counting a larger number of survival cells. For the experimental set I obvious changes in survival cells were not observed on the bare glass chamber with *E. coli* suspension under either room light (sample IA) or UV LED irradiation (sample IB). This indicates that the weak UV light alone used in this experiment did not affect the bacteria growth. In contrast, the survival cells (using 10^{-7} cfu/mL sample) decreased on the TiO_2/Au coating under room light (most of the time is in a dark incubator, sample IC) or UV LED light (sample ID). The efficiency is remarkably high and fast, as most of the bacteria were killed in 5 min. There are not enough survival cells for an accurate counting after 5 min. In the second set of experiments (set II), a higher concentration of bacterial suspensions of *E. coli* cells in 10^{-5} cfu/mL was used. Ideally, for having an accurate colony counting, the plate that is chosen for counting the survival cells should be in the range of 30−300 colonies on the plate, and be expected to have no survival cells in 60 min of illumination. Similar results on the two control samples were obtained: no obvious changes in cell survival for glass slides without TiO_2/Au coatings and under either room light (sample IIA) or UV LED irradiation (sample IIB). However,

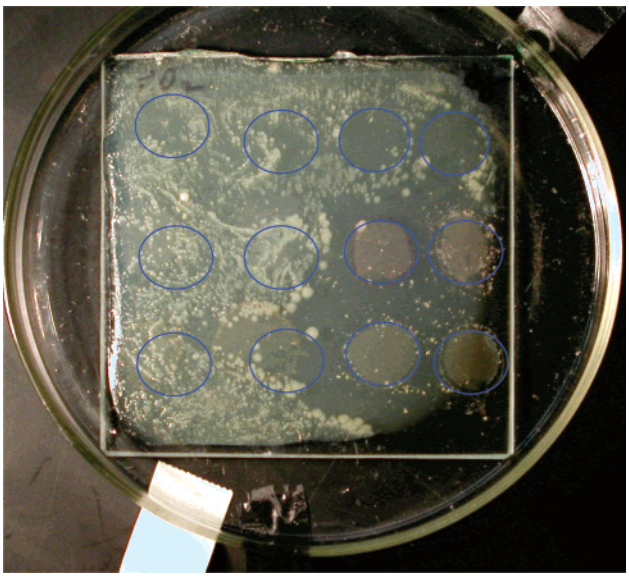

Figure 11. Antibacterial testing for *E. coli* on coated glass slide sprayed with different nanocomposites. See text for the conditions of coating.

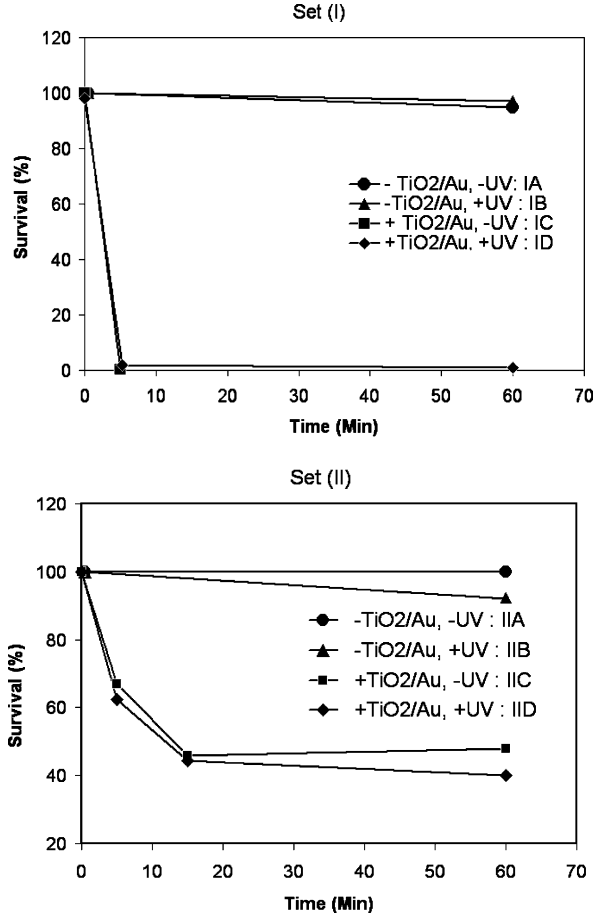

Figure 12. Changes in the survival of *E. coli* bacterial colonies on a TiO_2/Au nanocomposite coating. Set I and set II experiments were conducted by using a concentration of bacterial suspensions of *E. coli* cells in 10^{-7} and 10^{-5} cfu/mL, respectively.

the survival rate on the TiO_2/Au coating under a UV intensity of 1 mW/cm^2 LED source (sample IID) was almost the same as that on the coating under room light (sample IIC). This result is the same as the previous testing in aqueous solutions. This demonstrates that the nanosize anatase TiO_2 with Au-capped composites made in an acidic medium possesses photocatalytic activity even under room light or very weak UV illumination. The problem in this experiment was that, using a concentration of 10^{-5} cfu/mL dilution, there were over 800 colonies on each plate; a counting error could be the major problem responsible for the inaccurate data. However, the results showed that the gold-capped TiO_2 composite coating exhibited good photo-induced antibacterial effect for the sterilization of *E. coli*.

4. Conclusion

In this study, a novel and simple method was developed for the synthesis of highly photocatalytic, nanostructured, anatase TiO_2 particles in aqueous solution by hydrolysis of titanium isopropoxide in an acidic environment. Two different acids, $HClO_4$ and HNO_3, used as catalysts in the hydrolysis process were investigated. The results of characterization of the TiO_2 nanoparticles by UV−vis absorption spectroscopy, XRD, TEM, and AFM demonstrated that fairly uniform sized nanoparticles of 10−15 nm diameter with spherical-shaped anatase form were successfully obtained. There was no influence on the TiO_2 phase by the acid type used in this preparation method.

Moreover, the gold-capped TiO_2 nanocomposites were successfully synthesized with a mixture of TiO_2 solution and a noble metal salt ($HAuCl_4$) by both a chemical reduction method and a photoreduction method. The TEM images showed the gold-capped TiO_2 nanoparticles produced in this work had a very well-defined shape and small size. The ratio of [TiO_2]:[Au] directly affected the particle size and stability of the nanocomposites. Aggregation effects were observed with a [TiO_2]:[Au] ratio of 1:1 as indicated by TEM imaging. In contrast, the nanocomposites with a [TiO_2]:[Au] ratio of 20:1 were stable and a thin gold shell was formed with no significant change in particle size compared to the TiO_2 nanoparticles. Different percentages of vanadium-doped TiO_2 nanoparticles were also successfully prepared to extend the wavelength of TiO_2 from the UV to the visible region. The V-doped TiO_2 samples showed a red shift in the UV−vis absorption spectrum.

The antibacterial effect of those TiO_2 nanoparticles, gold-capped TiO_2 naonocomposites, and V-doped TiO_2 nanoparticles evaluated on two types of bacteria, *E. coli* and *B. megaterium*, were shown visually for the first time. The method to demonstrate the antibacterial effect of those nanoparticles in two forms, an aqueous phase and thin coating substrates, were successfully developed. Results showed good inhibition on two types of bacteria, *E. coli* and *B. megaterium*, even under room light. A decrease in the survival ratio of *E. coli* and a fast killing effect were observed. The results indicated the TiO_2 and gold-capped TiO_2 nanocomposites prepared in this study possess strong oxidizing ability and photocatalytic activity. The good antibacterial effect (60−100% killing efficiency as observed in Figure 12) may be due to those particles' small size, large surface area, large band gap energy, and more active sites for carrying out catalytic reactions. Further testing on the survival ratio of *E. coli* and *B. megaterium* (or other microorganisms) with the TiO_2, gold-capped TiO_2, and V-doped TiO_2 nanoparticles dispersed in coating formulations and coated glasses (or other substrates) is in progress.

References and Notes

(1) Sunada, K.; Watanabe, T.; Hashimoto, K. *Environ. Sci. Technol.* **2003**, *37*, 4785−4789.
(2) Jacoby, W. A.; Maness, C. P.; Wolfrum, E. J.; Blake, D. M.; Fennel, J. A. *Environ. Sci. Technol.* **1998**, *32*, 2650−2653.
(3) Linkous, A. C.; Carter, G. J.; Locuson, D. B.; Ouellette, A. J.; Slattery, D. K.; Simitha, L. A. *Environ. Sci. Technol.* **2000**, *34*, 4754−4758.
(4) Sunada, K.; Kikuchi, Y.; Hashimoto, K.; Fuhishima, A. *Environ. Sci. Technol.* **1998**, *32*, 726−728.
(5) Wolfrum, E. J.; Huang, J.; Blake, D. M.; Maness, P.; Huang, Z.; Fiest, J. *Environ. Sci. Technol.* **2002**, *36*, 3412−3419.
(6) Hagfeldt, A.; Gratzel, M. *Chem. Rev.* **1995**, *95*, 49−68.
(7) Murakami, Y.; Matsumoto, J.; Takasu, Y. *J. Phys. Chem. B* **1999**, *103*, 1836−1840.
(8) Alivisatos, A. P. *J. Phys. Chem.* **1996**, *100*, 13226−13239.
(9) Henglein, A. *J. Phys. Chem.* **1993**, *97*, 5457−5471.
(10) Kamat, V. P. *Chem. Rev.* **1993**, *93*, 267−300.
(11) Linsebigler, A. L.; Lu, G.; Yates, J. T. *Chem Rev.* **1995**, *95*, 735−738.
(12) Dawson, A.; Kamat, P. V. *J. Phys. Chem. B* **2001**, *105*, 960−966.
(13) Yu, C. J.; Zhang, L.; Zheng, Z.; Zhao, J. *Chem. Mater.* **2003**, *15*, 2280−2286.
(14) Martin, S. T.; Morrison, C. L.; Hoffman, M. R. *J. Phys. Chem.* **1994**, *98*, 13695−13704.
(15) Haick, H.; Paz, Y. *J. Phys. Chem. B* **2003**, *107*, 2319−2326.
(16) Hoffman, M. R.; Martin, S. T.; Choi, W.; Bahnemann, D. W. *Chem. Rev.* **1995**, *95*, 69−96.
(17) Stallings, W. E.; Lamb, H. *Langmuir* **2003**, *19*, 2989−2994.
(18) Peiro, A. M.; Peral, J.; Domingo, C.; Domenech, X.; Ayllon, J. *Chem. Mater.* **2001**, *13*, 2567−2573.
(19) Mogyorosi, K.; Dekany, I.; Fendler, H. J. *Langmuir* **2003**, *19*, 2938−2946.
(20) Hamid, A. M.; Rahman, A. I. *Malaysian J. Chem.* **2003**, *5* (1), 086−091.
(21) Park, I.; Jang, S.; Hong, S. J.; Vittal, R.; Kim, K. *Chem. Mater.* **2003**, *15*, 4633−4636.

(22) Tsevis, A.; Spanos, N.; Koutsoukos, P. G.; Van, A. L. J.; Lyklema, J. *J. Chem Soc., Faraday Trans.* **1998**, *94* (2), 295−300.

(23) Scalfani, A.; Palmisano, L.; Schiavello, M. *J. Phys. Chem.* **1990**, *94*, 829−832.

(24) Andersson, M.; Osterlund, L.; Ljungstrom, S.; Palmqvist, A. *J. Phys. Chem. B* **2002**, *106*, 10674−10679.

(25) Addamo, M.; Augugliaro, V.; Paola, A. D.; Garcia-Lopez, E.; Loddo, V.; Marci, G.; Molinari, R.; Palmisano, L.; Schiavello, M. *J. Phys. Chem. B* **2004**, *108*, 3303−3310.

(26) Zanella, R.; Giorgio, S.; Henry, R. C.; Louis, C. *J. Phys. Chem. B* **2002**, *106*, 7634−7642.

(27) Subranmanian, V.; Wolf, E. E.; Kamat, V. P. *Langmuir* **2003**, *19*, 469−474.

(28) Yu, C. J.; Yu, J.; Ho, W.; Jiang, Z.; Zhang, L. *Chem. Mater*. **2002**, *14*, 3808−3816.

(29) Choi, W.; Termin, A.; Hoffmann, M. R. *J. Phys. Chem.* **1994**, *98*, 13669−13679.

(30) Klosek, S.; Raftery, D. *J. Phys. Chem. B* **2001**, *105*, 2815−2819.

(31) Tortora, G.; Funke, R. B.; Case, L. C. *Microbiology; An Introduction*; Addison-Wesley Longman, Inc.: New York, 2001.

(32) Blake, M. D.; Manesss, P.; Huang, Z.; Wolfrun, J. E.; Huang, J. *Sep. Purif. Methods* **1999**, *28* (1), 1−50.

(33) Lu, Z.; Zhou, L.; Zhang, Z.; Shi, W.; Xie, Z.; Xie, H.; Pang, D.; Shen, P. *Langmuir* **2003**, *19*, 8765−8768.